Lifetime and hyperfine splitting measurements on the $7s$ and $6p$ levels in rubidium

E. Gomez, S. Aubin, L. A. Orozco,* and G. D. Sprouse

*Department of Physics and Astronomy, State University of New York, Stony Brook,
Stony Brook, New York 11794-3800*

We present lifetime measurements of the $7S_{1/2}$ level and the $6p$ manifold of rubidium. We use a time-correlated single-photon counting technique on a sample of ^{85}Rb atoms confined and cooled in a magneto-optic trap. The upper state of the $5P_{1/2}$ repumping transition serves as the resonant intermediate level for two-photon excitation of the $7s$ level. A probe laser provides the second step of the excitation, and we detect the decay of atomic fluorescence to the $5P_{3/2}$ level at 741 nm. The decay process feeds the $6p$ manifold that decays to the $5s$ ground state emitting UV photons. We measure lifetimes of 88.07 ± 0.40 and 120.7 ± 1.2 ns for the $7S_{1/2}$ level and $6p$ manifold, respectively; the hyperfine splitting of the $7S_{1/2}$ level is 282.6 ± 1.6 MHz. The agreement with theoretical calculations confirms the understanding of the wave functions involved and provides confidence on the possibility of extracting weak interaction constants from a parity nonconservation measurement. © 2004 Optical Society of America

OCIS codes: 300.6210, 020.4900, 020.4180, 020.7010.

1. INTRODUCTION

The lifetime of an excited level and its hyperfine splitting are properties related to the electronic wave functions of an atom. The lifetime, through the matrix elements of allowed transitions, probes the wave functions at large radii; hyperfine splitting samples their value at the nucleus. The comparison of the two types of measurement with theoretical predictions tests the quality of the computed wave functions. Calculations of the wave functions have now reached new levels of sophistication[1,2] based on many-body perturbation theory (MBPT). The calculations are particularly important in the interpretation of precision tests of discrete symmetries in atoms: parity nonconservation (PNC) (see, for example, the Cs measurements of Wood *et al.*[3,4]) and time reversal.[5]

We present our measurements on ^{85}Rb atoms in a magneto-optic trap (MOT) using time-correlated single-photon counting techniques. We measure the lifetimes of the $7s\ ^2S_{1/2}$ level and the $6p$ manifold as well as the hyperfine splitting of the $7s\ ^2S_{1/2}$ level. The work complements and aids the program of Fr spectroscopy and weak interaction physics.[6] We carry out all the Fr measurements in a trapped and cooled atomic gas. Rb and Fr have similar properties, and the same trap can be used to capture either of them by selection of the appropriate wavelengths.[7] Having the ability to trap both atoms helps us understand better our experimental results. The trap is optimized for Fr and it works on line with the superconducting Linear Accelerator at Stony Brook. Our Rb measurements are necessary to understand fully the systematic effects on our measurements of the equivalent levels in Fr, $9s$, $8p$.[8,9]

The Rb measurements presented here are an important test of MBPT calculations in a regime in which relativistic effects are not as important as in heavier atoms such as Fr. Measurements of excited-state atomic lifetimes in low-lying states of the s and p manifolds enhance our understanding of the wave functions and the importance of correlation corrections in their calculation.

We present the lifetime measurements in Section 2, detail the hyperfine splitting measurement in Section 3, and summarize the research within the context of similar measurements for Rb and Fr in Section 4.

2. LIFETIME MEASUREMENTS

A. Lifetime and Matrix Elements
The lifetime of a quantum mechanical system depends on the initial and final states wave functions and the dominant interaction. Since the electromagnetic interaction in atomic physics is well understood, radiative lifetimes provide information about atomic structure.

Lifetime τ of an excited state is related to partial lifetimes τ_i associated with each of the allowed decay channels by

$$1/\tau = \sum_i 1/\tau_i. \qquad (1)$$

The matrix element associated with a partial lifetime between two states connected by an allowed dipole transition is given by[10]

$$\frac{1}{\tau_i} = \frac{4}{3} \frac{\omega^3}{c^2} \alpha \frac{|\langle J||r||J'\rangle|^2}{2J' + 1}, \qquad (2)$$

where ω is the transition energy divided by $\hbar$, c is the speed of light, α is the fine-structure constant, J' and J are, respectively, the initial and final state angular mo-

menta, τ_i is the excited-state partial lifetime, and $|\langle J||r||J'\rangle|$ is the reduced matrix element.

Calculation of the radial matrix elements requires the wave functions of the initial and final states involved in the decay. The contributions of the wave function at a large distance become more important because of the presence of a radial operator. Knowledge of the atomic lifetimes and branching ratios in Rb determine the radial matrix elements for the transitions.

B. Sample Preparation

We used a high-efficiency MOT to capture a sample of Rb atoms at a temperature lower than 300 μK.[7] We loaded the MOT from a Rb vapor produced by a dispenser in a glass cell coated with a dry film. The MOT consists of three pairs of retroreflected beams, each with 15-mW/cm^2 intensity, 6-cm diameter ($1/e^2$ intensity), and red detuned 19 MHz from the atomic resonance. A pair of coils generates a magnetic field gradient of 6 G/cm. We trapped 10^5 atoms with a diameter of 0.2 mm and a typical lifetime between 5 and 10 s.

Figure 1 shows the energy levels of ^{85}Rb relevant for the trap, lifetime, and hyperfine splitting measurements. The trapping and cooling were done with a Coherent 899-21 titanium:sapphire (Ti:sapphire) laser at 780 nm between the $5S_{1/2}F = 3$ and the $5P_{3/2}F = 4$ levels. We repumped the atoms that fell out of the cycling transition with a Coherent 899-01 Ti:sapphire laser at 795 nm between the $5S_{1/2}F = 2$ and the $5P_{1/2}F = 3$ levels. A Coherent 899-21 Ti:sapphire probe laser at 728 nm com-
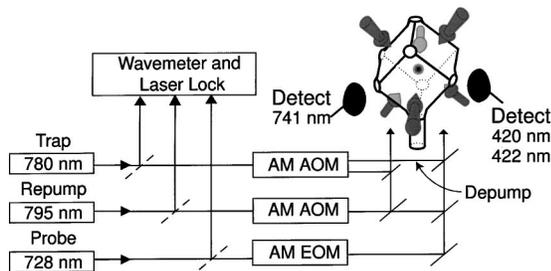
Fig. 3.   Decay paths for the $7s$ and $6p$ levels of ^{85}Rb.

pletes the two-photon transition. We used a depumper pulse at 780 nm between the $5S_{1/2}F = 3$ and the $5P_{3/2}F = 3$ levels before the two-photon transition to remove the atoms from the cycling transition and into the lower hyperfine ground state.

We excited the atoms in the trap to the $7s$ level by using a two-photon transition through the $5P_{1/2}$ level. To increase the population transfer to the $7s$ level we split the repumper light into two paths: one going directly to the trap with a large beam size to optimize the trapping efficiency and combining the other with the depumper and probe laser focused on the trap to optimize the excitation. We sent 12 mW of probe power, 9 μW of depumper power, and 2 mW of repumper power focused to a spot size between 1 and 3 mm to increase the excitation intensity.

Figure 2 shows the schematic of the laser system. We control the power of the lasers going into the trap with acousto-optic modulators (AOMs) and electro-optic modulators (EOMs). We measured the wavelength of the lasers with a Burleigh WV-1500 wavemeter. We locked the trap laser to ^{85}Rb by using saturation spectroscopy. We avoided long-term frequency drifts on the probe and repumper lasers by transferring the long-term stability of a He–Ne laser to the two lasers by means of a computer-controlled scanning Fabry–Perot cavity.[11]

The $7s$ level has four different electric (E1) dipole allowed decay channels as shown in Fig. 3. We detected the direct decay channel from the $7s$ to the $5P_{3/2}$ level at 741 nm to obtain the lifetime of the $7s$ level. The $7s$ level can also decay to the $6p$ level and from there cascade down to the $5s$ level, emitting a photon at 420 (or 422) nm in this last step. We collected the fluorescence at 420 (or 422) nm that contains contributions from the lifetime of the $7s$ and $6p$ levels. Using the results obtained for the lifetime of the $7s$ level we can extract a lifetime for the $6p$ manifold.

C. Experimental Method

We used the technique of time-correlated single-photon counting to measure the lifetimes.[12] This method has been used in the past to measure lifetimes of atoms in beams,[13] vapor cells,[14] and single ions.[15] Our group has used it to measure the lifetime of the $7p$, $7d$, and $9s$ levels in Fr (Refs. 8, 9, 16, and 17) and of the $5p$ levels in Rb.[16]

Fig. 1.   Energy levels of ^{85}Rb for trapping and two-photon excitation to the $7s$ level (solid lines) fluorescence detection (dashed lines) and undetected fluorescence (dotted lines).

Fig. 2.   Schematic of the trap: AM EOM, amplitude modulation with an electro-optic modulator, AM AOM, amplitude modulation with an acousto-optic modulator.

The cycle of the measurement has a repetition rate of 100 kHz controlled with a Berkeley Nucleonics Corp. BNC 8010 pulse generator and two Stanford Research Systems DG535 pulse delay generators as shown in Fig. 4. The cycle starts with 0.7 μs for state preparation. To do this we first removed the atoms from the cycling transition and inserted them into the lower hyperfine ground level with a depumper beam at 780 nm between the $5S_{1/2}F = 3$ and the $5P_{3/2}F = 3$ levels; see a in Fig. 1. Once there, the atoms were excited with the repumper laser to the $5P_{1/2}F = 3$ level; see b in Fig. 1. From there the probe laser took them to the $7S_{1/2}F = 3$ level; see c in Fig. 1. We detected fluorescence for 1.6 μs while the counting gate is on and kept all the lasers off during the last 1.3 μs. We used the rest of the cycle (8 μs) for cooling and trapping of atoms. At the beginning of the cycle we turned off the trap laser with a Crystal Technology 3200-144 AOM. The trap beam was focused to a transverse line in the AOM with a cylindrical lens telescope to avoid damage to the crystal while maintaining a large diffraction efficiency. This gives a 10:1 on/off ratio for the trap laser in 260 ns. We allowed an extra 240 ns to increase the on/off ratio for the trap laser before we excited the atoms to the $7s$ level for 200 ns. We turned off the probe with two Gsänger LM0202 EOMs and a Crystal Technology 3200-144 AOM. The two EOMs gave a fast turnoff for the probe laser and the AOM improved the long-term on/off ratio. The turnoff of the probe laser can be approximated with a half-Gaussian function with a FWHM of 7 ns. We obtained an on/off ratio of 600:1 after 20 ns. The fast turnoff of the EOMs creates strong rf emission. The photomultiplier tube (PMT) amplifiers can pick this emission and create false detection pulses. We minimized these false events by enclosing the EOMs and drivers inside a metallic cage in a separate room. Another Crystal Technologies 3200-144 AOM turned off the repumper simultaneously with the probe. We looked for fluorescence from the $7s$ level and the $6p$ manifold for 1.3 μs. We turned the trapping beams back on for the
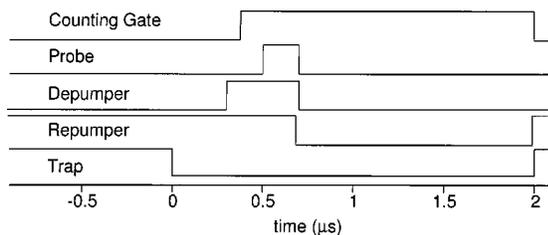
Fig. 4. Timing sequence for the excitation of atoms to the $7s$ level: high level is on, low level is off.
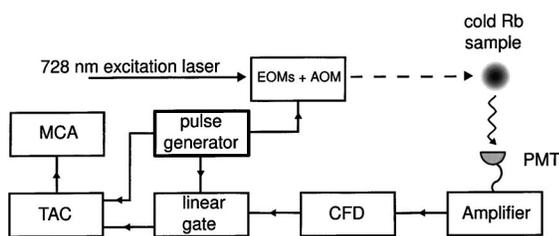
Fig. 5. Block diagram for the electronics used for the detection of $7s$ or $6p$ photons.

rest of the cycle and then repeated the entire cycle continuously for the duration of the measurement.

A 1:1 imaging system ($f/3.9$) collects the fluorescence photons onto a Roper Scientific MicroMax 1300YHS-DIF charge-coupled device camera. We monitored the trap with an interference filter at 780 nm in front of the camera. A beam splitter in the imaging system sends 50% of the light onto a PMT (Hamamatsu R636). An interference filter at 741 nm in front of the PMT reduced the background light other than fluorescence from the $7S_{1/2}$ to the $5P_{3/2}$ level. Another independent 1:1 imaging system ($f/3.5$) monitored the fluorescence from the $6p$ manifold to the $5S_{1/2}$ level with an interference filter at 420 nm (10-nm bandwidth at 50%) and an Amperex XP 2020Q PMT.

Figure 5 is a block diagram of the electronics used in the detection and processing of $7s$ and $6p$ photon events. The heart of the electronics is the time-to-amplitude converter (TAC) (Ortec 467 for the $7s$ photons and Ortec 437 for the $6p$ photons). The TAC receives a start and a stop pulse and outputs a voltage proportional to the time separation between pulses. The pulse generator used to control the timing of the lasers provided the stop pulse at a fixed delay from the lasers turnoff. A detected fluorescence photon provided the start pulse. Only one photon can be processed per cycle. The photon pulse generated by the PMT goes through some processing before it reaches the TAC. It first goes through an Ortec AN106/N amplifier and then to an Ortec 934 constant fraction discriminator (CFD). The output of the discriminator is a pulse of fixed shape with a constant time delay from the input pulse. The pulse then goes through an Ortec LG101/N linear gate that is open only during the excitation and fluorescence part of the cycle. Starting the TAC with a fluorescence photon eliminates the cycles with no detected photons. A histogram of the output of the TAC in a multichannel analyzer (MCA) (EG&G Trump-8k for the $7s$ photons and Canberra 3502 for the $6p$ photons) displays the exponential decay directly in real time.

We calibrated the MCA by replacing the start pulse given by the PMT with an electronic pulse generated by the pulse generator. We changed the separation between the start and the stop pulses in steps of 100 ns and fitted the resulting signal to determine both the linearity and the calibration. We verified the uniformity of the MCA channels by triggering the PMT with random photon events from room light. The result is a uniformly flat signal consistent with zero slope.

D. $7s$ Level Analysis
We measured the lifetime of the $7s$ level through its decay to the $5P_{3/2}$ level. We kept the number of atoms in the trap low (approximately 10^5) to reduce density-related effects (diameter of the trap of $\sim$0.2 mm). We operated with the number of detected photons per cycle to be much smaller than one and applied a small correction to the data to account for preferential counting of early events.[12] This correction appears when we have more than one photon per cycle. The correction, called pulse pileup correction, is given by

$$\mathcal{N}'_i = \frac{\mathcal{N}_i}{1 - \dfrac{1}{n_E}\sum_{j<i}\mathcal{N}_j}, \qquad (3)$$

where $\mathcal{N}_i$ is the number of counts in channel i of the MCA, n_E is the total number of cycles, and $\mathcal{N}'_i$ is the corrected number of counts for channel i. We typically get one count every 100 cycles (or 1 ms), which corresponds to a correction of less than 1% for the number of counts per channel.

Figure 6 shows the exponential decay obtained for a 47-min accumulation along with the fit and residuals. For times before -200 ns the small signal comes from trapping laser light leakage through the interference filter. Between $t = -200$ and $t = 0$ ns, we turned on the excitation beams (probe and depumper) that give the fast rise and plateau on the signal coming from both the fluorescence of the atoms and the leakage from the two additional lasers. When $t = 0$ ns, we turned all the laser beams off and the only light that remained was the fluorescence from the atoms. The fit starts 20 ns after the beams are turned off and stops when the signal is equal to the background. The fitting function is

$$S_{7s} = c_a \exp(-t/\tau) + c_b + c_m t, \qquad (4)$$

where t is the time (or channel number) and τ and $c_i\,(i = a,b,m)$ are the fitting constants. We obtained a background signal by repeating the experiment without atoms. The lifetime fit is affected slightly by the presence of a linear background that we include in the fit. The slope of the background is approximately two counts per 1000 channels per 1000 s of accumulation and comes from the slow turnoff of the trap laser. This particular decay has a reduced χ^2_ν of 1.07, where the noise in the
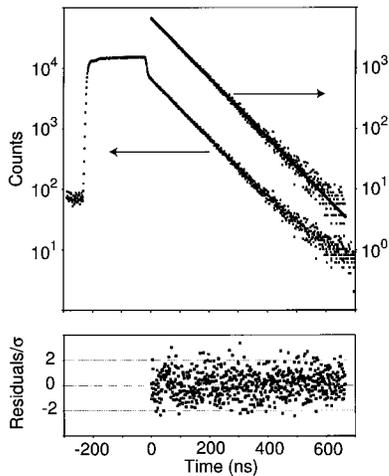
Fig. 6. Exponential decay of the $7s$ level. The upper plot contains the raw data that show the excitation turnon and turnoff as well as the exponential decay of the atoms (left scale). It also shows the background subtracted signal together with the exponential fit (right scale). The lower plot shows the normalized residuals (assuming statistical noise).

number of counts is statistical ($\sqrt{S}$). A discrete Fourier transform of the residuals shows no structure.

1. Systematic Effects

We searched for systematic effects by varying one experimental parameter at a time and looking for an effect on the obtained lifetime. Each measurement lasts for approximately 3000 s. First we studied the effects that the external variables have on the lifetime. Each measurement was obtained under slightly different conditions. We fitted them independently by using the fitting function of Eq. (4) and made a correlation study between the obtained lifetime and the external variable for each case.

Excitation pulse duration. We changed the excitation pulse duration between 100 and 800 ns. The lifetime is independent of the initial conditions of the decay. Changing the pulse duration can modify the initial conditions for the decay.

Probe intensity. We varied the probe intensity by a factor of 10, which is another way in which we can modify the initial conditions for the decay.

Magnetic field. The presence of a magnetic field from the MOT could influence the measured lifetime mainly through quantum beats between the Zeeman sublevels. We changed the magnetic field gradient from 4 to 7 G/cm.

Number of atoms. We changed the number of atoms from 6×10^4 to 1×10^7. Increasing the number of atoms increases the density and produces more collisions between the atoms as well as permits radiation trapping. These two effects will modify the lifetime. The photon detection rate also increases with the atom number. This rate becomes too high for the electronics of the MCA and the repetition rate for the experiment has to be reduced to 10 kHz, with a larger pulse pileup correction.

We quantify the correlation between the measured lifetime and the external variables by calculating the linear correlation coefficient. The integral of the probability distribution associated with the linear correlation coefficient provides the degree of correlation of the data with the external variable. A small value for the integral probability means significant correlation. In all the above cases the integral probability of the linear correlation coefficient is larger than 5%, which is consistent with no correlation. We keep the number of atoms low for all the measurements to avoid systematic effects related to collisions or to pulse pileup. Radiation trapping can be ignored because of the small population in the $5P_{3/2}$ level.

Other effects can influence the measurement but they are not related to a simple variable as above. In this case we make a reference measurement and then we modify something to test each of the above potential effects to obtain another measurement. We fit each independent data file using Eq. (4) and perform a χ^2 test to the obtained lifetimes to determine if they are consistent with statistical fluctuations.

Repumper turnoff. We looked for an effect of an imperfect turnoff of the repumper light by leaving the repumper on continuously. The repumper is used as the first step of the two-photon transition, and, when combined with an imperfect turnoff of the probe laser, it can introduce a false signal.

Hyperfine level. To our accuracy level, the lifetime

should be independent of the hyperfine level. We changed the initial hyperfine level of the decay; that is, instead of preparing the atoms in the $7S_{1/2}F = 3$ state we prepared them in the $7S_{1/2}F = 2$ state.

Electronics. We looked for effects related to electronic components by interchanging the MCA for the $7s$ and $6p$ detection systems. It is important to keep the Canberra MCA count rate low.

Probe turnoff. An imperfect extinction of the probe laser will show up as an excess in the initial data points of the decay. This effect can be revealed by changing the initial and final point for the fit. The spread of the lifetimes as a function of the starting point of the fit is consistent with the statistical uncertainty. There is no dependence on the final point for the fit within our statistical precision.

All the above measurements give an integral probability for χ^2 between 5% and 95%, which is consistent with statistical fluctuations.

Trap displacement. We displaced the trap keeping the magnetic field fixed, such that the atoms sample a different magnetic environment. To move the trap position we inserted a piece of glass in front of one of the retroreflection mirrors in the MOT. We repeated the same procedure for the three retroreflection mirrors in the MOT. The MOT image on the camera shows trap displacements smaller than one trap diameter in the transverse direction to the camera, and we have no information on the longitudinal displacement. This is a complex systematic effect since it involves the change of several experimental parameters such as alignment of the excitation lasers. This makes it difficult to assign a single parameter responsible for the variations we observe. We tried differ-
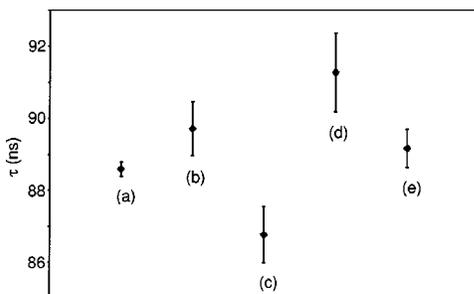
Fig. 7. Lifetime obtained when the trap is displaced by the insertion of a piece of glass in the retroreflection mirrors of the MOT while the magnetic field environment remains unchanged: (a) no displacement and displacement using (b) mirror 1, (c) mirror 2, (d) mirror 3 and beams realigned, (e) no displacement and beams not realigned.

Table 1. Error Budget for $7s$ Level Lifetime Measurements

Error	Percent
Statistical	± 0.17
Trap displacement	± 0.38
Time calibration	± 0.01
TAC/MCA nonlinearity	± 0.04
Quantum beats	$< \pm 0.10$
Total	± 0.43
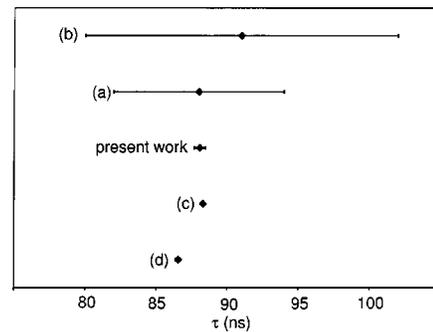
Fig. 8. Experimental result of the $7s$ lifetime in Rb together with previous experimental results from (a) Marek and Munster[20] and (b) Bulos *et al.*,[21] and theoretical predictions from (c) Safronova *et al.*[18] and (d) Theodosiou.[19]

ent combinations of moving the trap with and without realignment. The integral probability of χ^2 shows fluctuations larger than statistical. We included an uncertainty contribution of $\pm 0.38\%$, equal to the dispersion of the lifetime values (Fig. 7).

Quantum beats. We looked for quantum beats in the residuals of the fit. A discrete Fourier transform of the residuals shows no structure. The value of $\pm 0.1\%$ quoted for the uncertainty due to quantum beats comes from a theoretical calculation with a simple model that assumes well-defined Zeeman sublevels as in the presence of a uniform magnetic field. The presence of a magnetic field gradient further reduces the quantum beat contribution.

Some of the information obtained can be extended to measurements in Fr. Changing the number of atoms is complicated in Fr so we can use the results for Rb to determine if we are working in a good regime. Both atoms have a similar atomic structure, so most tests should give similar results. The most important difference is their sensitivity to magnetic effects because of the difference in multiplicity of Zeeman sublevels and hyperfine separation.

2. Result and Comparison with Theory

The average of the reduced χ_ν^2 of the individual files is 1.04 ± 0.08. The different lifetimes from the fit were averaged to obtain the final result. The lifetime of the $7s$ level is 88.07 ± 0.38 ns. A fit to the file that results from adding all the files gives consistent results. Table 1 summarizes the error budget for the experiment.

Figure 8 is a comparison of our result with theoretical predictions[18,19] for the lifetime of the $7s$ level as well as previous measurements.[20,21] Theoretical calculations reach a level of precision below 1%.[22] An experimental verification of this precision is important to increase the confidence in such calculations. This information is crucial to extract weak interaction physics from PNC experiments. The prediction from *ab initio* calculations for the $7s$ level lifetime is 88.3 ns.[18] The agreement shows the remarkable level of sophistication of atomic structure calculations.

E. $6p$ Level Analysis

The $7s$ level has the four decay channels shown in Fig. 3. We detect the indirect decay from the $6p$ to the $5s$ levels

to obtain information about the $6p$ level. The atoms that decay from the $6p$ level come from a cascade decay from the $7s$ level and the decay cannot be described with a single exponential. The signal from this indirect decay is the sum of three exponential functions with lifetimes corresponding to the $7S_{1/2}$, $6P_{1/2}$, and $6P_{3/2}$ levels. We can make use of the result obtained in the previous section for the lifetime of the $7S_{1/2}$ level to measure the lifetime of the $6p$ manifold. Here we present the analysis of the $6p$ signal that contains contributions from the two fine levels. The fine separation of the $6p$ levels in Rb is 1.4 nm, which is smaller than the 10-nm transmission width of the interference filter. In the case of Fr, the fine separation of the corresponding levels is larger, and we use interference filters to resolve both contributions seperately.[8,9]

The lifetimes of the two fine $6p$ levels are expected to be similar. We assume that the decay signal is given by the sum of two exponential functions, one for the $7s$ level and the other for the $6p$ level, so that the fitting function is

$$S_{6p} = A_b + A_{7s}\exp(-t/\tau_{7s}) + A_{6p}\exp(-t/\tau_{6p}), \quad (5)$$

where τ_{7s} is the lifetime of the $7s$ level obtained in Subsection 2.D, and τ_{6p}, A_b, A_{7s}, and A_{6p} are the fitting constants. Figure 9 shows the signal obtained for a single file and the resulting curve if we subtract the background and the exponential contribution from the $7s$ level. This last curve corresponds to the exponential decay of the $6p$ manifold. We use files only with low count rates to avoid systematic effects associated with the slow response of the MCA.

The lifetime we obtained for the $6p$ manifold depends on the value of the lifetime of the $7s$ level. The uncertainty in the $7s$ lifetime influences the precision with which we can extract the $6p$ lifetime. The probability distribution for τ_{6p} is given by
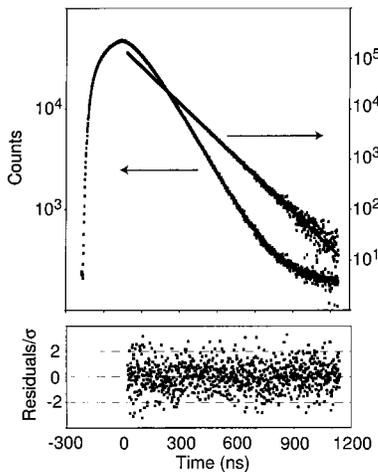
Fig. 9. Decay of the $6p$ manifold. The upper plot contains the raw data (left scale) and the data minus the background minus the exponential contribution from the $7s$ level (right scale). An exponential fit to this last curve is also shown. The lower plot contains the normalized residuals (assuming statistical noise).

Table 2. Error Budget for $6p$ Manifold Lifetime Measurements

Error	Percent
Statistical	± 0.15
$7s$ uncertainty propagation	± 0.25
Time calibration	± 0.94
Total	± 0.98

$$P(\tau'') = \int \mathrm{d}\tau' \frac{1}{\sqrt{2\pi}\sigma_{7s}} \exp\left[-\frac{1}{2}\left(\frac{\tau' - \tau_{7s}}{\sigma_{7s}} \right)^2 \right] \frac{1}{\sqrt{2\pi}\sigma_{6p}(\tau')}$$
$$\times \exp\left\{ -\frac{1}{2}\left[\frac{\tau'' - \tau_{6p}(\tau')}{\sigma_{6p}(\tau')} \right]^2 \right\}. \quad (6)$$

The integrand contains two Gaussian distributions: the first gives the probability distribution for the $7s$ level lifetime centered on τ_{7s} with an uncertainty σ_{7s} and the second gives the probability distribution for the $6p$ manifold lifetime centered on $\tau_{6p}(\tau')$ with an uncertainty $\sigma_{6p}(\tau')$. We assume a value of τ' for the lifetime of τ_{7s} and include that in the fitting function [Eq. (5)] to obtain a value for $\tau_{6p}(\tau')$. We repeated the same procedure for different values of τ' and performed the integral of Eq. (6).

The result for the integral when τ_{6p} and σ_{6p} do not strongly depend on τ' gives approximately $\tau_{6p} = \tau_{6p}(\tau_{7s}) = 120.7$ ns and

$$\sigma_{6p} = \left\{ \sigma_{6p}(\tau_{7s})^2 + \left[\frac{\mathrm{d}\tau_{6p}(\tau')}{\mathrm{d}\tau'}\sigma_{7s} \right]^2 \right\}^{1/2} = 0.35 \text{ ns},$$

as confirmed by numerical integration. This result assumes uncorrelated errors for the individual files used for the fit but includes the spread brought by systematic checks on the $7s$ level lifetime. The uncertainty in the MCA calibration is at the 0.94% level. Table 2 summarizes the error budget that gives a final result for the lifetime of the $6p$ manifold of 120.7 $\pm$ 1.2 ns.

We can make a comparison between the predicted and the measured signals to give some bounds on the possible values for the lifetime of each fine level. The decay signal is obtained by solving the following rate equations:

$$\frac{\mathrm{d}N_s}{\mathrm{d}t} = -\frac{N_s}{\tau_s},$$

$$\frac{\mathrm{d}N_{p1}}{\mathrm{d}t} = B_{p1}\frac{N_s}{\tau_s} - \frac{N_{p1}}{\tau_{p1}},$$

$$\frac{\mathrm{d}N_{p3}}{\mathrm{d}t} = B_{p3}\frac{N_s}{\tau_s} - \frac{N_{p3}}{\tau_{p3}}, \quad (7)$$

where N_i and τ_i give the population and lifetime, respectively, of level i, with $i = s$, $p1$, $p3$ representing the $7S_{1/2}$, $6P_{1/2}$, and $6P_{3/2}$ levels, and $B_{p1} = 0.132$, $B_{p3} = 0.255$ the theoretical branching ratios from the $7S_{1/2}$ level to the $6P_{1/2}$ and $6P_{3/2}$ levels, respectively.[18] To solve Eqs. (7) we need the initial conditions for the level populations at the beginning of the decay (or equivalently at the end of the excitation pulse). Figure 6 shows that during the excitation the population of the $7s$ level reaches a steady state quickly. We assume that the $7s$ population

is constant during the excitation pulse. We also assume that before excitation we have no population in the $6p$ level. With these assumptions we can calculate the population of the $6p$ levels during excitation given by

$$N_{p1} = N_s B_{p1} \frac{\tau_{p1}}{\tau_s} [1 - \exp(-t/\tau_{p1})],$$

$$N_{p3} = N_s B_{p3} \frac{\tau_{p3}}{\tau_s} [1 - \exp(-t/\tau_{p3})]. \qquad (8)$$

The excitation lasts for $T = 200$ ns, so evaluation of these expressions after this time will give the initial conditions for the decay. Solving Eqs. (7) with these initial conditions gives the population of the three levels as a function of time. The signal measured by the PMT is proportional to the sum of the decay rates of each of the $6p$ levels to the $5s$ level. The underlying assumption that the response of the PMT and the interference filter is the same for both $6p$ levels is reasonable because of the small energy separation between them (1.4 nm). The signal ($\widetilde{S_{6p}}$) coming from the PMT is given by

$$\widetilde{S_{6p}} = \widetilde{A_b} + \widetilde{A}\left(b_{p1} \frac{N_{p1}}{\tau_{p1}} + b_{p3} \frac{N_{p3}}{\tau_{p3}} \right),$$

$$= \widetilde{A_b} + \widetilde{A}'\left\{ \left(\frac{b_{p1} B_{p1}}{\tau_s - \tau_{p1}} + \frac{b_{p3} B_{p3}}{\tau_s - \tau_{p3}} \right) \exp(-t/\tau_s) \right.$$

$$+ b_{p1} B_{p1} \left[\frac{1 - \exp(-T/\tau_{p1})}{\tau_s} - \frac{1}{\tau_s - \tau_{p1}} \right]$$

$$\times \exp(-t/\tau_{p1})$$

$$+ b_{p3} B_{p3} \left[\frac{1 - \exp(-T/\tau_{p3})}{\tau_s} - \frac{1}{\tau_s - \tau_{p3}} \right]$$

$$\left. \times \exp(-t/\tau_{p3}) \right\}, \qquad (9)$$

where $b_{p1} = 0.194$ and $b_{p3} = 0.236$ are the branching ratios for the decays from the $6P_{1/2}$ and $6P_{3/2}$ levels to the $5s$ level, respectively,[18] and $\widetilde{A_b}$, $\widetilde{A}$, and $\widetilde{A}'$ are the background and scale constants.

To compare Eq. (9) with Eq. (5) we need to combine the two exponential functions for the $6p$ levels into a single function since we do not have enough resolution to separate them; that is, we need to make

$$b_{p1} B_{p1} \left[\frac{1 - \exp(-T/\tau_{p1})}{\tau_s} - \frac{1}{\tau_s - \tau_{p1}} \right] \exp(-t/\tau_{p1})$$

$$+ b_{p3} B_{p3} \left[\frac{1 - \exp(-T/\tau_{p3})}{\tau_s} - \frac{1}{\tau_s - \tau_{p3}} \right]$$

$$\times \exp(-t/\tau_{p3}) \sim C \exp(-t/\tau'_{6p}). \qquad (10)$$

Expression (10) will be equal in the least-squares sense, meaning that we will solve for the values of C and τ'_{6p} that minimize the square of the difference of the two sides of the equation in the range from 0 to ∞. The theoretical values for the $6p$ fine level lifetimes are $\tau_{p1} = 129$ ns and $\tau_{p3} = 118$ ns.[18] Using these values we obtain the following expression for the signal:
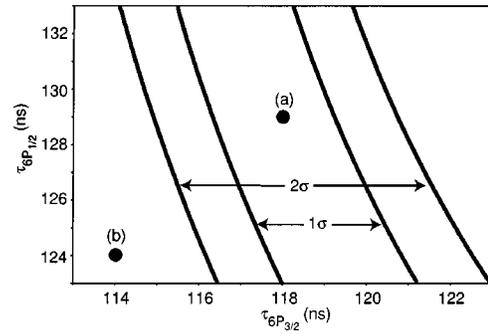
Fig. 10. Constraints on the lifetimes of the two $6p$ fine levels in Rb by use of the model described in the text and the experimental result. The solid curves define the limits of the 1σ and 2σ regions. The circles represent theoretical predictions from (a) Safronova *et al.*[18] and (b) Theodosiou.[19]

$$\widetilde{S_{6p}} = \widetilde{A_b} + \widetilde{C}[\exp(-t/\tau_s) - 1.29 \exp(-t/\tau'_{6p})], \quad (11)$$

with $\tau'_{6p} = 120.7$ ns. The ratio of the amplitudes of the $7s$ and $6p$ exponential functions is fixed by Eq. (9). Using the fitting parameters from Eq. (5) for the experimental result we obtain $A_{6p}/A_{7s} = -1.44 \pm 0.01$. The difference between the predicted ratio and the one obtained is 12%.

We can invert the previous procedure to set limits on the possible values of the $6p$ fine level lifetimes. If we take τ'_{6p} equal to the experimental value (or some other value) we can obtain only that value with specific combinations of τ_{p1} and τ_{p3}. This will not fix either τ_{p1} or τ_{p3}, but it will create a functional relation between the two. Figure 10 gives the 1σ and 2σ bands for the experimental result by use of the method described in which the branching ratios are assumed to be constant. The theoretical predictions are also included in Fig. 10, and the *ab initio* calculation[18] is in agreement with the experimental result that includes the statistical and calibration uncertainty.

3. HYPERFINE SPLITTING

A. Hyperfine Splitting and Matrix Elements
The hyperfine splitting in an atom is produced by interaction of electrons with a nuclear magnetic moment. The hyperfine splitting constant for an s state is given by[23]

$$A = \frac{8\pi}{3} \frac{\mu_0 \mu_B}{4\pi h} 2g \mu_N |\psi(0)|^2 \kappa, \qquad (12)$$

where μ_0 is the magnetic constant, μ_B is the Bohr magneton, μ_N is the nuclear magneton, g is the nuclear g factor, and κ is a correction term that includes the relativistic correction, the Breit correction, and the Bohr–Weisskopf effect. The hyperfine splitting constant works as a probe for the magnetic environment created by electrons at the nucleus. Measurements of hyperfine splitting tests the wave functions at short distances. The experimental setup used for the lifetime measurements gives the flexibility to reach both of the $7s$ hyperfine levels. We have a clean detection method for the number of atoms promoted to the $7s$ level through the fluorescence

photons from the $7s$ level or from the $6p$ manifold. Here we present the results for the measurement of the hyperfine splitting of the $7s$ level.

B. Experimental Method

We measured the hyperfine splitting of the $7s$ state by scanning the frequency of the probe laser and by counting the number of photons as a function of frequency. The excitation sequence corresponds to the one used for the lifetime measurement with the excitation pulse length increased to 1.5 μs. We monitored the wavelength of the probe laser with a wavemeter (Burleigh WV-1500) that has a resolution of ± 30 MHz. We improved the measurement resolution with a Fabry–Perot cavity that acts as a frequency ruler. We sent the probe laser and a frequency-stabilized Melles–Griot He–Ne laser (05-STP-901) into a Fabry–Perot cavity that is constantly scanning. We detected and digitized the transmitted intensity. A computer monitors the position of the transmission peak of the probe laser relative to two transmission peaks of the He–Ne laser. Using this method we controlled the drift of our lasers to less than 1 MHz/h.[11] As we scanned the probe laser, its relative position with respect to the He–Ne laser peaks changes and can even move to a neighboring free spectral range. Knowledge of the free spectral range of the cavity gives us a ruler with which to measure frequency differences.

We calibrated the cavity with a New Focus 4002 EOM driven with a signal generator (Gigatronics 1026) to add sidebands of known frequency to the probe laser before it enters the cavity. We selected the probe laser frequency equal to one of the hyperfine levels and the frequency driving the EOM about half of the hyperfine splitting, such that the second-order sideband is close to the other hyperfine level. A scan of the sideband frequency around this value gives a local cavity calibration to 0.15%.

The method for detection of fluorescence photons is the same as the one used for the lifetime measurement (Fig. 5) with the TAC and MCA replaced by a gate and delay generator (Ortec 416A) to create positive pulses and a multichannel scaler (National Instruments BNC 2090) to count the number of detected photons per second.

C. Analysis and Results

The resolution of the wavemeter can be improved if one assumes that the noise is Gaussian. Figure 11 shows a plot of the number of photons versus wavemeter reading. The origin is arbitrarily defined to be 13732.476 cm^{-1} on the wavemeter. We fit the data with two Gaussian peaks plus a background. With this method we found a hyperfine separation of 277.3 ± 5.4 MHz.

We performed several scans recording both the number of counts and the relative (or percent) position of the laser transmission peak with respect to two fixed He–Ne transmission peaks on the cavity. The result of a typical scan is shown in Fig. 12. The two peaks correspond to the two hyperfine levels and are separated by one free spectral range. We fitted each peak with a Lorentzian function plus a background and then averaged over all the scans. The difference in position between the two peaks is compared against the calibration to obtain the separation in

megahertz. The statistical uncertainty is the main contribution to the error budget (Table 3) with a 0.46% contribution.

The presence of a magnetic field could modify the hyperfine splitting measurement through Zeeman splitting of the magnetic sublevels. Assuming that all the atoms start from a common state and reach the highest magnetic sublevel on each of the hyperfine levels, we obtained an upper limit for the contribution of the Zeeman shift of 0.16%. The presence of laser beams on the excitation can induce an ac shift and splitting of the hyperfine levels. We do not observe any clear asymmetry or splitting on each of the hyperfine peaks, although we do see some power broadening. The natural linewidth from the lifetime is 11.4 MHz, whereas the data have a linewidth of 24 MHz, which shows power broadening. We modeled the scan signal by solving the steady-state optical Bloch equations[24] and obtained a spectrum consistent with the data (Fig. 13). The intensities and detunings of the
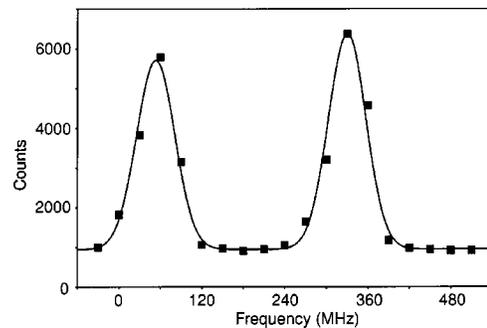
Fig. 11. Scan with wavemeter reading. The dots represent the number of photons per second and the solid curve is a fit with two Gaussian functions plus a background. The origin is arbitrarily defined to be 13732.467 cm^{-1} on the wavemeter.
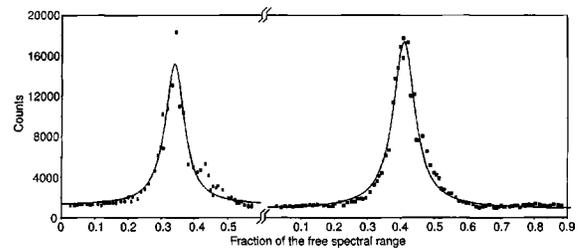
Fig. 12. Scan with the cavity reading. The horizontal axis is the relative (or percent) position of the probe laser transmission peak with respect to two fixed He–Ne transmission peaks in the cavity. The dots represent the number of photons per second and the solid curve is a fit with a Lorentzian function plus a background. The two peaks correspond to the two hyperfine levels and are separated by one free spectral range.

Table 3. Error Budget for $7s$ Level Hyperfine Splitting Measurements

Error	Percent
Statistical	± 0.46
Cavity calibration	± 0.15
Differential Zeeman shift	± 0.16
Stark ac asymmetrical broadening	$< \pm 0.20$
Total	± 0.55
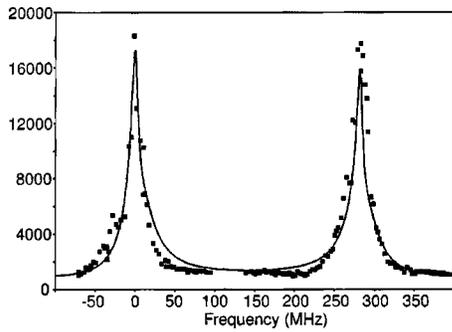
Fig. 13. Solution of the steady-state optical Bloch equations and its comparison with the data. The intensities and detunings of the beams were adjusted to approximate the data and are consistent with the experimental values. We also add a background and an overall scale to the simulation. The probe intensity used is 27 mW/cm^2, the repumper intensity is 37 mW/cm^2, and the repumper detuning is 3 MHz.
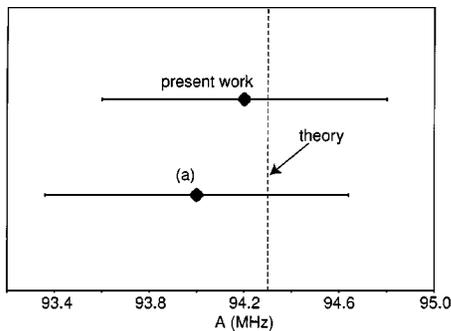
Fig. 14. Result for the hyperfine constant measurement and comparison with (a) previous experimental results[25] and theoretical prediction[26] (dotted line).

beams were adjusted to approximate the data and are consistent with the experimental ones. Using this model, we set limits to less than 0.2% for the effect of the ac Stark shift on the hyperfine splitting. Table 3 summarizes the error budget for the measurement. We found a hyperfine splitting for the 7s level of 282.6 ± 1.6 MHz.

The relation between the hyperfine shift and the magnetic dipole hyperfine constant (A) for an s level is given by

$$\frac{E_{\mathrm{HF}}}{h} = A\frac{K}{2},\qquad(13)$$

with $K = F(F + 1) - I(I + 1) - J(J + 1)$. In our case $I = 5/2$ and $J = 1/2$ so we have $A = 94.2 \pm 0.6$ MHz. Figure 14 shows a comparison of the present work with previous experiments[25] and a theoretical prediction.[26] The theoretical prediction assumes a nuclear magnetic moment of 1.3534 in units of μ_N, the nuclear magneton. We found good agreement between both experimental results and theory. Measurements of the hyperfine splitting of an s level are useful to understand the contributions from radiative corrections such as the one produced by the Breit interaction.[27]

4. CONCLUSIONS

We have measured the lifetime and hyperfine splitting of the second excited $S_{1/2}$ level of Rb and the lifetime of the second excited p manifold of Rb. We used two-photon excitation and time-correlated single-photon counting techniques on a sample of cold ^{85}Rb atoms confined in a MOT. Our 7s lifetime measurement has excellent statistics, but the result is limited by systematic uncertainties. The measurement represents a tenfold improvement in accuracy from previous measurements. The lifetime measurement test calculations of radial matrix elements that connect excited states in Rb. Comparisons with *ab initio* calculations of the matrix elements for different decay channels agree to better than 0.3%. The measurement of the lifetime of the 6p manifold does not differentiate between the two decay channels from the fine structure and achieves less accuracy, whereas a comparison with theory is model dependent but sets bounds for the two contributions. The 0.57% hyperfine splitting measurement is in agreement with previous values and theoretical calculations.

All these measurements confirm the high quality predictions of MBPT calculations and increase the confidence in the methods applied to heavier alkali atoms such as Fr and Cs for similar spectroscopic studies and extraction of weak interaction information from PNC measurements.

REFERENCES

1. W. R. Johnson, M. S. Safronova, and U. I. Safronova, "Combined effect of coherent Z exchange and the hyperfine interaction in the atomic parity-nonconserving interaction," Phys. Rev. A **67**, 062106 (2003).
2. J. S. M. Ginges and V. V. Flambaum, "Violations of fundamental symmetries in atoms and tests of unification theories of elementary particles," Phys. Rep. **397**, 63–154 (2004).
3. C. S. Wood, S. C. Bennett, D. Cho, B. P. Masterson, J. L. Roberts, C. E. Tanner, and C. E. Wieman, "Measurement of parity nonconservation and an anapole moment in cesium," Science **275**, 1759–1763 (1997).
4. C. S. Wood, S. C. Bennett, J. L. Roberts, D. Cho, and C. E. Wieman, "Precision measurement of parity nonconservation in cesium," Can. J. Phys. **77**, 7–75 (1999).
5. S. K. Lamoreaux and I. B. Khriplovich, *CP Violation without Strangeness* (Springer-Verlag, New York, 1997).
6. L. A. Orozco, "Spectroscopy with trapped francium," in *Trapped Particles and Fundamental Physics*, S. N. Atutov, R. Calabrese, and L. Moi, eds., Vol. 51 of NATO Science Series: II: Mathematics, Physics, and Chemistry (Kluwer Academic, Dordrecht, The Netherlands, 2002), pp. 125–159.
7. S. Aubin, E. Gomez, L. A. Orozco, and G. D. Sprouse, "High efficiency magneto-optical trap for unstable isotopes," Rev. Sci. Instrum. **74**, 4342–4351 (2003).
8. S. Aubin, E. Gomez, L. A. Orozco, and G. D. Sprouse, "Lifetime measurement of the 9s level of atomic francium," Opt. Lett. **28**, 2055–2057 (2003).
9. S. Aubin, E. Gomez, L. A. Orozco, and G. D. Sprouse, "Lifetimes of the 9s and 8p levels of atomic francium," Phys. Rev. A (to be published).

10. R. D. Cowan, *Theory of Atomic Structure and Spectra* (University of California, Berkeley, Berkeley, Calif., 1981).
11. W. Z. Zhao, J. E. Simsarian, L. A. Orozco, and G. D. Sprouse, "A computer-based digital feedback control of frequency drift of multiple lasers," Rev. Sci. Instrum. **69**, 3737–3740 (1998).
12. D. V. O'Connor and D. Phillips, *Time-Correlated Single Photon Counting* (Academic, London, 1984).
13. L. Young, W. T. Hill III, S. J. Sibener, S. D. Price, C. E. Tanner, C. E. Wieman, and S. R. Leone, "Precision lifetime measurements of Cs $6p\,^2P_{1/2}$ and $6p\,^2P_{3/2}$ levels by single-photon counting," Phys. Rev. A **50**, 2174–2181 (1994).
14. B. Hoeling, J. R. Yeh, T. Takekoshi, and R. J. Knize, "Measurement of the lifetime of the atomic cesium $5\,^2D_{5/2}$ state with diode-laser excitation," Opt. Lett. **21**, 74–76 (1996).
15. R. G. DeVoe and R. G. Brewer, "Precision measurements of the lifetime of a single trapped ion with a nonlinear electro-optic switch," Opt. Lett. **19**, 1891–1893 (1994).
16. J. E. Simsarian, L. A. Orozco, G. D. Sprouse, and W. Z. Zhao, "Lifetime measurements of the $7p$ levels of atomic francium," Phys. Rev. A **57**, 2448–2458 (1998).
17. J. M. Grossman, R. P. Fliller III, L. A. Orozco, M. R. Pearson, and G. D. Sprouse, "Lifetime measurements of the $7D$ levels of atomic francium," Phys. Rev. A **62**, 062502 (2000).
18. M. S. Safronova, C. J. Williams, and C. W. Clark, "Relativistic many-body calculations of electric-dipole matrix elements, lifetimes, and polarizabilities in rubidium," Phys. Rev. A **69**, 022509 (2004).
19. C. E. Theodosiou, "Lifetimes of alkali-metal–atom Rydberg states," Phys. Rev. A **30**, 2881–2909 (1984).
20. J. Marek and P. Munster, "Radiative lifetimes of excited S states of rubidium up to quantum number $n = 12$," J. Phys. B **13**, 1731–1741 (1980).
21. B. R. Bulos, R. Gupta, and W. Happer, "Lifetime measurements in excited S states of K, Rb, and Cs by the cascade Hanle effect," J. Opt. Soc. Am. **66**, 426–433 (1976).
22. A. Derevianko, "Correlated many-body treatment of the Breit interaction with application to cesium atomic properties and parity violation," Phys. Rev. A **65**, 012106 (2002).
23. H. Kopfermann, *Nuclear Moments* (Academic, New York, 1958).
24. J. M. Grossman, R. P. Fliller III, Mehlstäubler, L. A. Orozco, M. R. Pearson, G. D. Sprouse, and W. Z. Zhao, "Energies and hyperfine splittings of the $7D$ levels of atomic francium," Phys. Rev. A **62**, 052507 (2000).
25. R. Gupta, W. Happer, L. K. Lam, and S. Svanberg, "Hyperfine-structure measurements of excited S states of the stable isotopes of potassium, rubidium, and cesium by cascade radio-frequency spectroscopy," Phys. Rev. A **8**, 2792–2810 (1973).
26. M. S. Safronova, W. R. Johnson, and A. Derevianko, "Relativistic many-body calculations of energy levels, hyperfine constants, electric-dipole matrix elements, and static polarizabilities for alkali-metal atoms," Phys. Rev. A **60**, 4476–4487 (1999).
27. O. P. Sushkov, "Breit-interaction correction to the hyperfine constant of an external s electron in a many-electron atom," Phys. Rev. A **63**, 042504 (2001).